

An Efficient and Integrated Algorithm for Video Enhancement in Challenging Lighting Conditions

Xuan Dong, Jiangtao (Gene) Wen, *Senior Member, IEEE*, Weixin Li, Yi (Amy) Pang, Guan Wang

Abstract—We describe a novel integrated algorithm for real-time enhancement of video acquired under challenging lighting conditions. Such conditions include low lighting, haze, and high dynamic range situations. The algorithm automatically detects the dominate source of impairment, then depending on whether it is low lighting, haze or others, a corresponding pre-processing is applied to the input video, followed by the core enhancement algorithm. Temporal and spatial redundancies in the video input are utilized to facilitate real-time processing and to improve temporal and spatial consistency of the output. The proposed algorithm can be used as an independent module, or be integrated in either a video encoder or a video decoder for further optimizations.

I. INTRODUCTION

As video surveillance equipments and mobile devices such as digital cameras, smart phones and netbooks are increasingly widely deployed, cameras are expected to acquire, record and sometimes compress and transmit video content in all lighting and weather conditions. The majority of cameras, however, are not specifically designed to be all-purpose and weather-proof, rendering the video footage unusable for critical applications under many circumstances.

Image and video processing and enhancement including gamma correction, de-hazing, de-blurring and etc. are well-studied areas with many successful algorithms proposed over the years. Although different algorithms perform well for different lighting impairments, they often require tedious and sometimes manual input-dependent fine-tuning of algorithm parameters. In addition, different specific types of impairments often require different specific algorithms.

Take the enhancement of videos acquired under low lighting conditions as an example. To mitigate the problem, far and near infrared based techniques ([1], [2], [3], [4]) are used in many systems, and at the same time, various image processing based approaches have also been proposed. Although far and near infrared systems are useful for detecting objects such as pedestrians and animals in low lighting environments, especially in “professional” video surveillance systems, they suffer from the common disadvantage that detectable objects must have a temperature that is higher than their surroundings. In many cases where the critical object has a temperature similar to its surroundings, e.g. a big hole in the road, the infrared systems are not as helpful. Furthermore, infrared

systems are usually more expensive, harder to maintain, with a relatively shorter life-span than conventional systems. They also introduce extra, and often times considerable power consumption. In many consumer applications such as video capture and communications on smart phones, it is usually not feasible to deploy infrared systems due to such cost and power consumption issues. Conventional low lighting image and video processing enhancement algorithms such as [5] and [6] often work by reducing noise in the input low lighting video followed by contrast enhancement techniques such as tone-mapping, histogram stretching and equalization, and gamma correction to recover visual information in low lighting images and videos. Although these algorithms can lead to very visually pleasing enhancement results, they are usually too complicated for practical real-time applications, especially on mobile devices. For example, the processing speed of the algorithm in [5] was only 6 fps even with GPU acceleration. In [6], recovering each single image required more than one minute.

In this paper, we describe a novel integrated video enhancement algorithm applicable to a wide range of input impairments. It has low computational and memory complexities that are both within the realm of reasonable availability of many mobile devices. In our system, a low complexity automatic module first determines the pre-dominant source of impairment in the input video. The input is then pre-processed based on the particular source of impairment, followed by processing by the core enhancement module. Finally, post-processing is applied to produce the enhanced output. In addition, spatial and temporal correlations were utilized to improve the speed of the algorithm and visual quality of the output, enabling it to be embedded into video encoders or decoders to share temporal and spatial prediction modules in the video codec to further lower complexity.

The paper is organized as the following. In Section II, we present the heuristic evidences that motivated the idea in this paper. In Section III, we explain the core enhancement algorithm in detail, while in Section IV we describe various algorithms for reducing the computational and memory complexities. Section V contains the experimental results. Given that in real-world applications, the video enhancement module could be deployed in multiple stages of the end to end procedure, e.g. before compression and transmission/storage, or after compression and transmission/storage but before decompression, or after decompression and before the video content displayed on the monitor, we examine the complexity and RD tradeoff associated with applying the proposed algorithm in these different steps in the experiments. Finally we conclude

Xuan Dong, Jiangtao (Gene) Wen and Yi (Amy) Pang are with the Computer Science Department, Tsinghua University, Beijing, China, 100084. Weixin Li and Guan Wang are with the School of Computer Science and Engineering, Beihang University, Beijing, China, 100191. E-mail: jtwen@tsinghua.edu.cn

the paper and future works in Section VI.

II. A NOVEL INTEGRATED ALGORITHM FOR VIDEO ENHANCEMENT

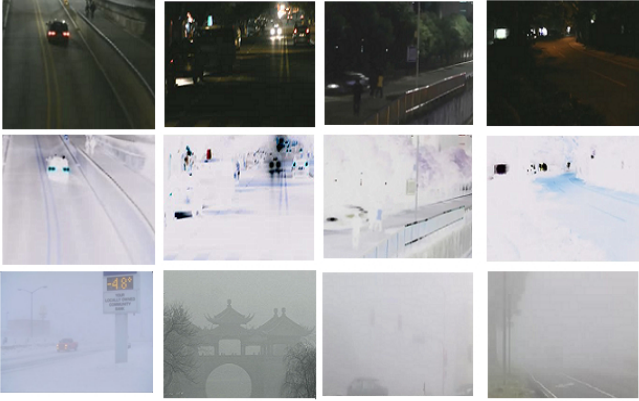


Fig. 1. Examples of original (Top), inverted low lighting videos/images (Middle) and haze videos/images (Bottom).

The motivation for our algorithm is a key observation that if we perform a pixel-wise inversion of low lighting videos or high dynamic range videos, the results look quite similar to hazy videos. As an illustrative example, we randomly selected (by Google) and captured a total of 100 images and video clips in haze, low lighting and high dynamic range weather conditions respectively. Some examples are shown in Fig. 1. Here, the “inversion” operation is simply

$$R^c(x) = 255 - I^c(x), \quad (1)$$

where $R^c(x)$ and $I^c(x)$ are intensities for the corresponding color (RGB) channel c for pixel x in the input and inverted frame respectively.

As can be clearly seen from Fig. 1, at least visually, the video in hazy weather are similar to the inverted output of videos captured in low lighting and high dynamic range conditions. This is intuitive because as illustrated in [7], in all these cases, e.g. hazy videos and low lighting videos, light captured by the camera is blended with the airlight (ambient light reflected into the line of sight by atmospheric particles). The only difference is the actual brightness of the airlight, white in the case of haze videos, black in the case of low lighting and high dynamic range videos.

The observation is confirmed by various haze detection algorithms. We implemented haze detection using the HVS threshold range based method [8], the Dark Object Subtraction (DOS) approach [9], and the spatial frequency based technique [10], and found that hazy, inverted low lighting videos and inverted high dynamic range videos were all classified as hazy video clips, as opposed to “normal” clips.

We also performed the chi-square test to examine the statistical similarities between hazy videos and inverted low lighting and high dynamic range videos. The chi-square test is a standard statistical tool widely used to determine if observed data are consistent with a specific hypothesis. As explained in [11], in chi-square tests, a p value is calculated, and usually,

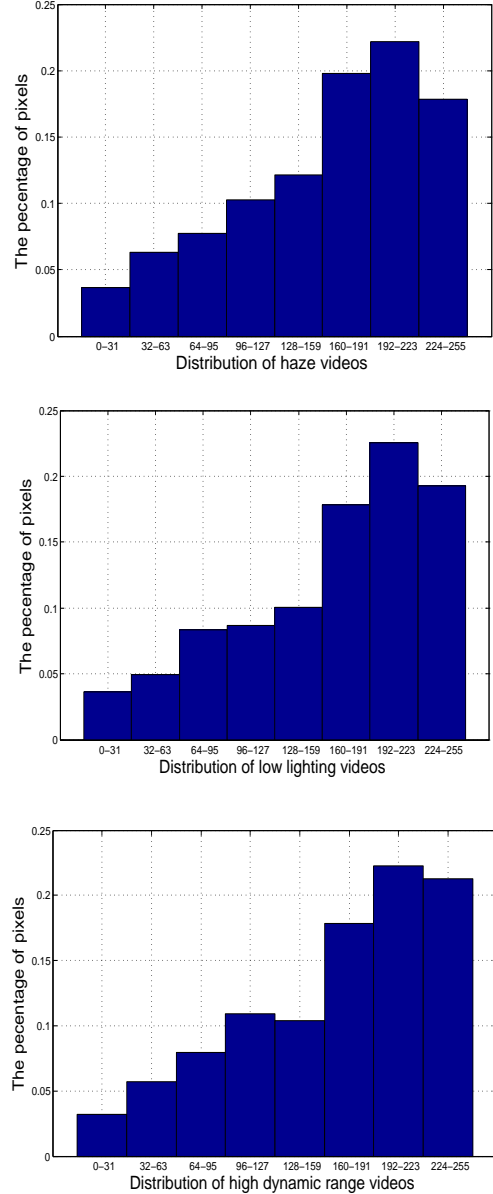


Fig. 2. The histogram of the minimum intensity of each pixel’s three color channels of haze videos (Top), low lighting videos (Middle) and high dynamic range videos (Bottom).

if $p > 0.05$, it is reasonable to assume that the deviation of the observed data from the expectation is due to chance alone. In our experiments, the expected distribution was calculated from hazy videos and the observed statistics from inverted low lighting and high dynamic range videos were tested. In the experiments, we divided the range $[0, 255]$ of color channel intensities into eight equal intervals, corresponding to a degree of freedom of 7. According to the chi-square distribution table, if we adopt the common standard of $p > 0.05$, the corresponding upper threshold for the chi-square value should be 14.07. The histogram of the minimum intensities of all color channels of all pixels for hazy videos, inverted low lighting and inverted high dynamic range videos were used in the tests, some examples are shown in Fig. 2. The results of the chi-

TABLE I
RESULTS OF CHI SQUARE TESTS

Data of chi square test	Degrees of Freedom	Chi square values
Haze videos and inverted low lighting videos	7	13.21
Haze videos and inverted high dynamic range videos	7	11.53



Fig. 3. Examples of hazy videos/images (Left) and their dark channel images (Right).



Fig. 4. Examples of low lighting videos/images (Left) and their dark channel images (Right).



Fig. 5. Examples of high dynamic range videos/images (Left) and their dark channel images (Right).

square tests are given in Table I. As can be seen from the table, the chi-square values are far smaller than 14.07, demonstrating that our hypothesis of the similarities between haze videos and inverted low lighting videos, and between haze videos and high dynamic range videos is reasonable.

Through the experiments, we also found that the pixels whose minimum intensity of the three color channels was low had a very high probability of locating in regions of houses, vehicles and etc.. We introduce the concept of Region of Interests (ROIs) for these regions. To visually demonstrate the ROIs, we calculated the image of minimum intensities of color channels for hazy videos, inverted low lighting videos and inverted high dynamic range videos. Three examples are shown in Fig. 3, Fig. 4 and Fig. 5.

In conclusion, through visual observation and statistical tests, we found that video captured in a number of challenging lighting conditions is statistically and visually similar to hazy videos. Therefore, it is conceivable that a generic core module could be used for the enhancement of all these cases.

III. A GENERIC VIDEO ENHANCEMENT ALGORITHM BASED ON IMAGE DE-HAZING

A. Core De-Hazing Based Enhancement Module

Since after proper pre-processing, videos captured in challenging lighting conditions, e.g. low lighting and high dynamic

range, exhibit strong similarities with hazy videos in both the visual and statistical domains, the core enhancement algorithm in our proposed system is an improved de-hazing algorithm based on [12].

As mentioned above, most of the existing advanced haze-removal algorithms ([13], [12], [14], and [15]) are based on the well-known degradation model proposed by Koschmieder in 1924 [7]:

$$R(x) = J(x)t(x) + A(1 - t(x)), \quad (2)$$

where A is the global airlight, $R(x)$ is the intensity of pixel x that the camera captures, $J(x)$ is the intensity of the original objects or scene, and $t(x)$ is the medium transmission function describing the percentage of the light emitted from the objects or scene that reaches the camera. This model assumes that each degraded pixel is a combination of the airlight and the unknown surface radiance. The medium transmission describes what percentage of the light emitted from the objects or scene can reach the camera. And it is determined by the scene depth and the scattering coefficient of the atmosphere. For the same video where the scattering coefficient of the atmosphere is constant, the light is more heavily affected by the airlight in sky regions because of the longer distance. In other regions such as vehicles, houses and etc., especially those nearby, the light is less affected by the airlight.

The critical part of all the algorithms based on the Koschmieder model is to estimate A and $t(x)$ from the recorded image intensity $I(x)$ so as to recover the $J(x)$ from $I(x)$. For example, in [13], Independent Component Analysis is used to estimate the medium transmission and the airlight. In [12], the medium transmission and airlight are estimated by the Dark Channel method, based on the assumption that the medium transmission in a local patch is constant.

In our system, we estimate $t(x)$ according to [12] using

$$t(x) = 1 - \omega \min_{c \in \{r, g, b\}} \left\{ \min_{y \in \Omega(x)} \frac{R^c(y)}{A^c} \right\}, \quad (3)$$

where $\omega = 0.8$ and $\Omega(x)$ is a local 9×9 block centered at x in this paper. As our system also targets application



Fig. 6. Examples of processing steps of low lighting enhancement algorithm: input image I (Top left), inverted input image R (Top right), haze removal result J of the image R (Bottom left), and output image (Bottom right).

in mobile devices, the cpu-and-memory-costly soft matting method proposed in [12] is not implemented in our algorithm.

To estimate airlight, we first note that the schemes in existing image haze removal algorithms are usually not robust and even very small changes to the airlight value might lead to very large changes to the recovered images or video frames. Therefore, calculating airlight frame-wise not only increases the overall complexity of the system, but also introduces visual inconsistency between frames, thereby creating annoying visual artifacts. Fig. 7 shows an example using the results of the algorithm in [12]. Notice the difference between the first and fourth frame in the middle row.

Based on this observation, we propose to calculate airlight only once for a Group of Pictures (GOP). This is done for the first frame of the GOP, then the same value is used for all subsequent frames in the same GOP. In the implementation, we also incorporated a scene change detection module so as to detect sudden changes in airlight that are not aligned with GOP boundaries but merit recalculation.

In our system, to estimate airlight, we first select 100 pixels whose minimum intensities in all color (RGB) channels are the highest in the image. Then from these pixels, we choose the single pixel whose sum of RGB values is the highest. Among successive GOPs, we refresh the value of airlight using the equation

$$A = A * 0.4 + A_t * 0.6, \quad (4)$$

where A_t is the airlight value calculated in this GOP, A is the global airlight value. This can efficiently avoid severe changes of the global airlight value A , bringing about the excellent recovered results and saving a large amount of computation at the same time. Examples of the recovered results are shown in Fig. 7. The first and fourth frame in the bottom row change gradually using our algorithm.

Then, from (2), we can find

$$J(x) = \frac{R(x) - A}{t(x)} + A. \quad (5)$$

Although (5) works reasonably well for haze removal, through experiments we found that direct application of equation (5) might lead to under-enhancement for low lighting areas and over-enhancement for high lighting areas when applied to low lighting video enhancement. To further optimize the calculation of $t(x)$, we focus on enhancing the ROIs while avoid processing the background, e.g. sky regions in low lighting and high dynamic range videos. This not only further reduces computational complexity, but also improves overall visual quality. To this end, we adjust $t(x)$ adaptively while maintaining its spatial continuity, so that the resulted video becomes more smooth visually. We introduce a multiplier $P(x)$ into equation (5), and through extensive experiments, we find that $P(x)$ can be set as

$$P(x) = \begin{cases} 2t(x) & 0 < t(x) \leq 0.5, \\ -2t^2(x) + 8 - \frac{3}{t(x)} & 0.5 < t(x) \leq 1. \end{cases} \quad (6)$$

Then (5) becomes

$$J(x) = \frac{R(x) - A}{P(x)t(x)} + A. \quad (7)$$

The idea behind (7) is as the following. When $t(x)$ is smaller than 0.5, which means that the corresponding pixel needs boosting, we assign $P(x)$ a small value to make $P(x)t(x)$ even smaller so as to increase the RGB intensities of this pixel. On the other hand, when $t(x)$ is greater than 0.5, we refrain from overly boosting the corresponding pixel intensity. When $t(x)$ is close to 1, $P(x)t(x)$ may be larger than 1, resulting in slight “dulling” of the pixel, so as to make the overall visual quality more balanced and pleasant.

For low lighting and high dynamic range videos, once $J(x)$ is recovered, the inversion operation (1) is performed again to produce the enhanced videos of the original input. This process is conceptually shown in Fig. 6. The improvement after introducing $P(x)$ can be seen in Fig. 9.

B. Automatic Impairment Source Detection

As mentioned above, we use the generic video enhancement algorithm of the previous subsection for enhancing video acquired in a number of challenging lighting conditions. In addition to this core enhancement module, the overall system also contains a module for automatically detecting the main source of visual quality degradation to determine if the pre-processing by pixel-wise inversion is required. In the case when pixel-wise inversion is required, different pixel wise fine tuning may also be introduced so that the eventual output after enhancement is further optimized. The flow diagram for this automatic detection system is shown in Fig. 8.

Our detection algorithm is based on the technique introduced by R. Lim et al. [8]. To reduce complexity, we only perform the automatic detection for the first frame in a GOP, coupled with a scene change detection. The corresponding algorithm parameters are shown in Table II. The test is conducted for each pixel in the frame. If the percentage of hazy

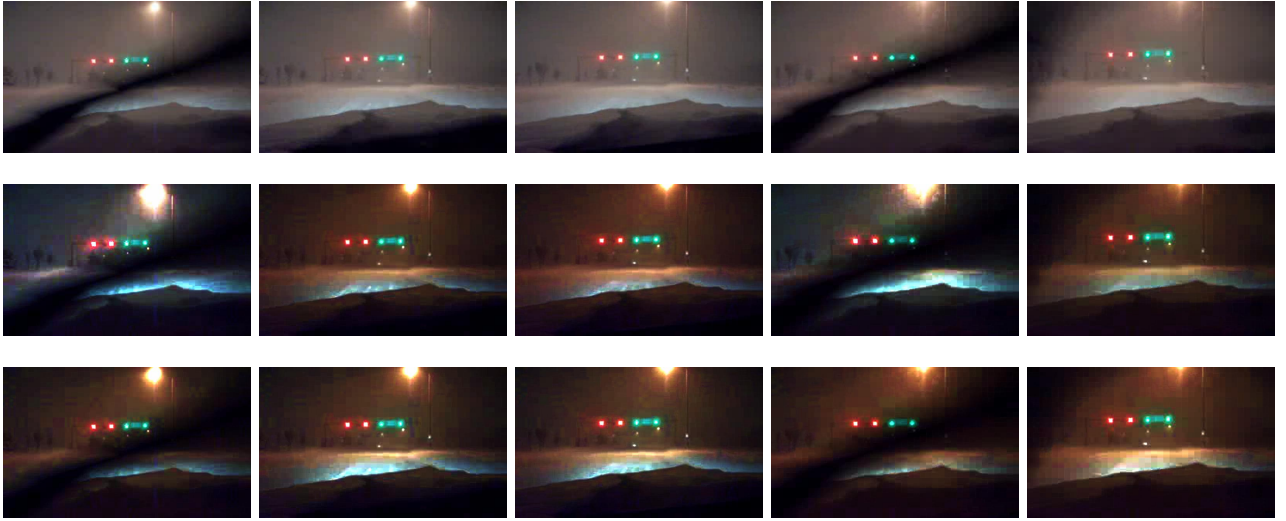


Fig. 7. The comparison of original, haze removal, and optimized haze removal video clips. Top: input video sequences. Middle: outputs of image haze removal algorithm of [12]. Bottom: outputs of haze removal using our optimized algorithm in calculating airlight.

TABLE II
SPECIFIC PARAMETERS OF THE HAZE DETECTION ALGORITHM.

	Color attribute	Threshold range
S	0 ~ 255	0 ~ 130
V	0 ~ 255	90 ~ 240

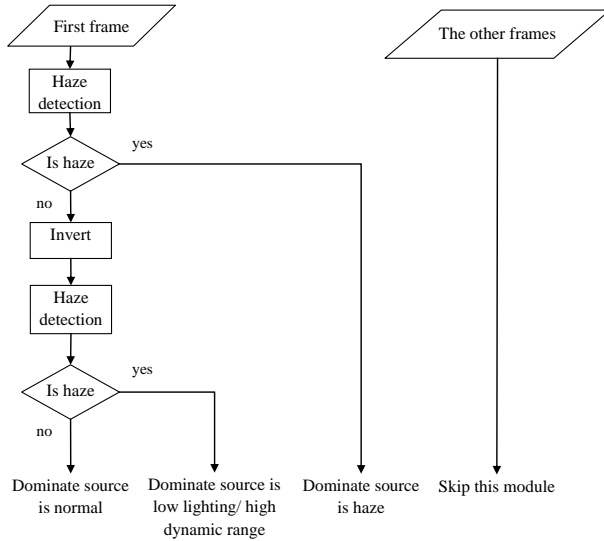


Fig. 8. Flow diagram of the module of determining dominant source of impairment.

pixels in a picture is higher than 60%, we consider the picture as a hazy picture. Similarly, if an image is determined to be a hazy picture after inversion, it is labeled as a low lighting or high dynamic range image, both of which require the introduction of the multiplier $P(x)$ into the core enhancement algorithm.

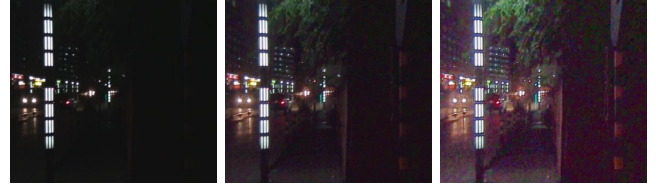


Fig. 9. Examples of optimizing low lighting and high dynamic range enhancement algorithm by introducing $P(x)$: Input (Left), output of the enhancement algorithm without introducing $P(x)$ (Middle), and output of the enhancement algorithm by introducing $P(x)$ (Right).

IV. ACCELERATION OF PROPOSED VIDEO ENHANCEMENT PROCESSING ALGORITHM

The algorithm described in Section III is a frame based approach. Through experimental results, we found that the calculation of $t(x)$ occupies about 60% of the total computation time. For real-time and low complexity processing of video inputs, it is not desirable to apply the algorithm of Section III on a frame by frame basis, which not only has high computational complexity, but also makes the output results much more sensitive to temporal and spatial noise, and destroys the temporal and spatial consistency of the processed outputs, thereby lower the overall perceptual quality.

To solve these problems, we notice that the $t(x)$ and other model parameters are correlated temporally and spatially. Therefore, we propose to accelerate the algorithm by introducing motion estimation.

Motion estimation/compensation (ME/MC) is a key procedure of the state-of-the-art video compression standards. By matching blocks in subsequently encoded frames to find the “best” match of a block to be encoded and a block of the same size that has already been encoded and then decoded (referred to as the “reference”), video compression algorithms use the reference as a prediction of the block to be encoded and encodes only the difference (termed the “residual”) between the reference and the block to be encoded, thereby reducing the rate that is required to encode the current block to a

fidelity level. The process of finding the best match between a block to be encoded and a block in a reference frame is called “motion estimation”, and the “best” match is usually determined by jointly considering the rate and distortion costs of the match. If a “best” match block is found, the current block will be encoded in inter mode and only the residual will be encoded. Otherwise, the current block will be encoded in intra mode. The most commonly used metric for distortion in motion estimation is the Sum of Absolute Differences (SAD).

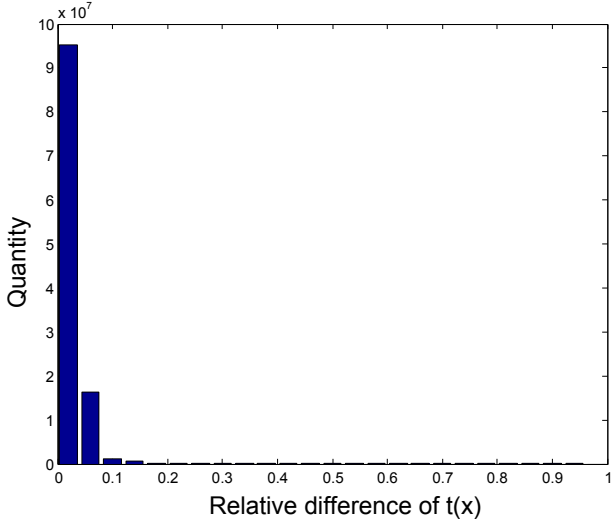


Fig. 10. Differences of $t(x)$ values between the predicted block’s pixels’ and its reference block’s pixels’.

To verify the feasibility of using temporal block matching and ME to expedite $t(x)$ calculation, we calculated the differences of $t(x)$ values for pixels in the predicted and reference blocks. The statistics in Fig. 10 shows that the differences are less than 10% in almost all cases. Therefore, we could utilize ME/MC to accelerate the computationally intensive calculation of $t(x)$ and only needed to calculate $t(x)$ of a few selective frames. For the non-critical frames, we used the corresponding $t(x)$ values of the reference pixels. To reduce the complexity of the motion estimation process, we used mature fast motion estimation algorithms e.g. *Enhanced Prediction Zonal Search (EPZS)* [16]. When calculating the SAD, similar to [17] and [18], we only utilized a subset of the pixels in the current and reference blocks using the pattern shown in Fig. 11. With this pattern, our calculation “touched” a total of 60 pixels in a 16×16 block, or roughly 25%. These pixels were located on either the diagonal or the edges, resulting in about 75% reduction in SAD calculation when implemented in software on a general purpose processor.

In our implementation, when the proposed algorithm is deployed prior to video compression or after video decompression, we first divide the input frames into GOPs. The GOPs could either contain a fix number of frames, or decided based on a max GOP size (in frames) and scene changing. Each GOP starts with an Intra coded frame (I frame), for which all $t(x)$ values are calculated. ME is performed for the remaining frames (P frames) of the GOP, similar to conventional video

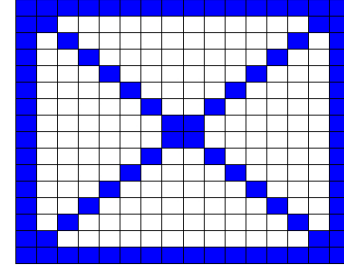


Fig. 11. Subsampling pattern of proposed fast SAD algorithm.

encoding. To this end, each P frame is divided into non-overlapping 16×16 blocks, for which a motion search using the SAD is conducted. A threshold T is defined for the SAD of blocks: if the SAD is below the threshold which means a “best” match block is found, the calculation of $t(x)$ for the entire MB is skipped. Otherwise, $t(x)$ still needs to be calculated. In both cases, the values for the current frame are stored for possible use for the next frame. The flow diagram is shown in Fig. 12. We call this acceleration algorithm as *ME acceleration enhancement algorithm*.

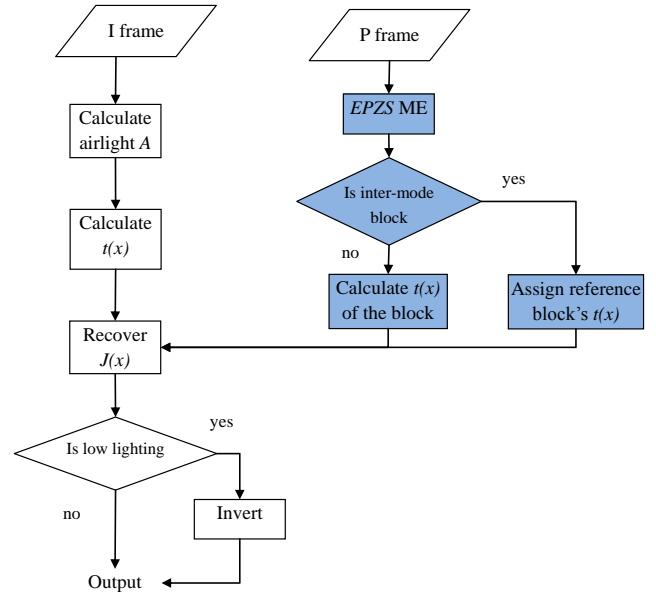


Fig. 12. Flow diagram of the core enhancement algorithm with ME acceleration.

In addition to operating as a stand-alone module with uncompressed pixel information as both the input and output, the ME accelerated enhancement algorithm could also be integrated into a video encoder or a video decoder. When the algorithm is integrated with a video encoder, the encoder and the enhancement can share the ME module. When integrated with the decoder, the system has the potential of using the motion information contained in the input video bitstream directly, and thereby by-passing the entire ME process. Such integration will usually lead to a RD loss. The reason for this loss is first and foremost that the ME module in the encoder with which the enhancement module is integrated or

the encoder with which the bitstreams that a decoder with enhancement decodes may not be optimized for finding the best matches in $t(x)$ values. For example, when the enhancement module is integrated with an decoder, it may have to decode an input bitstream encoded by a low complexity encoder using a really small ME range. The traditional SAD or SAD-plus-rate metrics for ME are also not optimal for $t(x)$ match search. However, through extensive experiments with widely used encoders and decoders, we found that such quality loss were usually small, and well-justified by the savings in computational cost. The flow diagrams of integrating the ME acceleration enhancement algorithm into encoder and decoder are shown in Fig. 15 and Fig. 16. Some of the comparisons can be found in Section V.

V. EXPERIMENTAL RESULTS

To evaluate the proposed algorithm, a series of experiments were conducted with a Windows PC (Intel Core 2 Duo processor running at 2.0 GHz with 3G of RAM) and an iPhone 4. The resolution of testing videos in our experiments was 640×480 .



Fig. 13. Examples of low lighting video enhancement algorithm: Original input (Top), and the enhancement result (Bottom).

Examples of the enhancement outputs for low lighting, high dynamic range and hazy videos are shown in Fig. 13, Fig. 14 and Fig. 17 respectively. As we can see from these figures, the improvements in visibility are obvious. In Fig. 13, the yellow light from the windows and signs such as “Hobby Town” and other Chinese characters were recovered in correct color. In Fig. 14, the headlight of the car in the original input made letters on the license plate very difficult to read. After enhancement with our algorithm, the license plate became much more intelligible. The algorithm also worked well for



Fig. 14. Examples of high dynamic range video enhancement algorithm: Original input (Top), and the enhancement result (Bottom).

video captured in hazy, rainy and snowy weathers as shown in Fig. 17, Fig. 18 and Fig. 19.

In addition, the proposed ME-based acceleration greatly reduces the complexity of the algorithm with little information lost. As mentioned above, there are three possible ways of incorporating ME into the enhancement algorithm, i.e. through a separate ME module in the enhancement system, as well as utilizing the ME module and information available in a video encoder or decoder. Some example outputs of the frame-wise enhancement algorithm and these three ways of incorporating ME are shown in Fig. 23, with virtually no visual difference. We also calculated the average RD curves of ten randomly selected experimental videos using the three acceleration methods. The reference was enhancement using the proposed frame-wise enhancement algorithm in YUV region. The RD curves of performing the frame-wise enhancement algorithm before encoding or after decoding are shown in Fig. 20, while the results for acceleration using a separate ME module are given in Fig. 21, and integrating the ME acceleration into the codec are shown in Fig. 22. As the RD curves in our experiments reflect the aggregated outcome of both coding and enhancement, and because enhancement was not optimized for PSNR based distortion, the shape of our RD curve looks different from RD curves for video compression systems, even though distortion as measured in PSNR is still a monotonic function of the rate. First, from the three figures, we find that in general, performing enhancement before encoding has better overall RD performance. Although enhancing after decoding means we can transmit un-enhanced video clips, which usually having lower contrast, less detail and are easier to compress, the reconstructed quality after decoder/enhancement is heavily

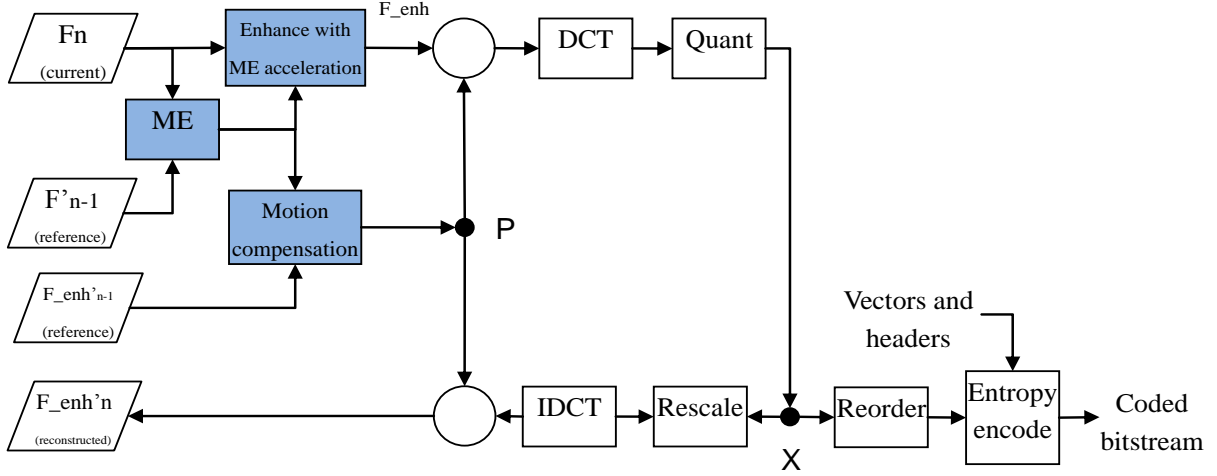


Fig. 15. Flow diagram of the integration of encoder and ME acceleration enhancement algorithm.

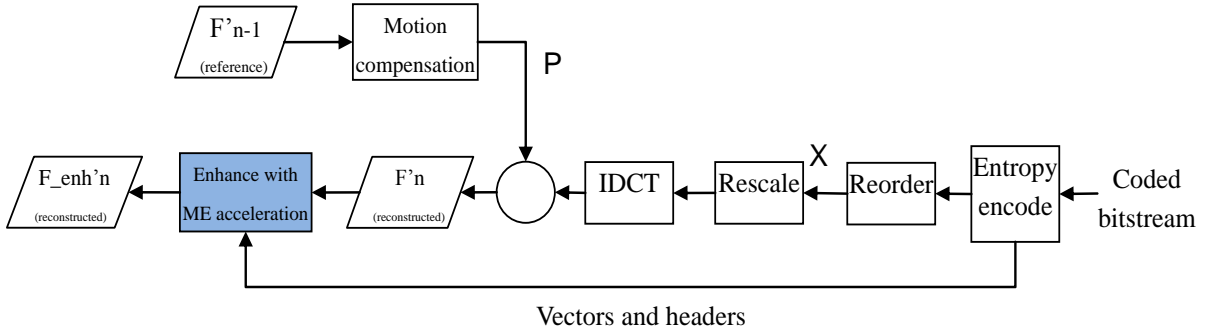


Fig. 16. Flow diagram of the integration of decoder and ME acceleration enhancement algorithm.

affected by the loss of quality during the encoding, leading to an overall RD performance loss of 2 dB for the cases in the experiments. In addition, in Fig. 20, the RD loss of frame-wise enhancement was due to encoding and decoding. In Fig. 21, the RD loss resulted from ME acceleration and encoding/decoding. In Fig. 21, the RD loss resulted from integration of ME acceleration algorithm into encoder and decoder. Overall however, the RD loss introduced by ME acceleration and integration was small in PSNR terms, and not visible subjectively.

We also measured the computational complexity of frame-wise enhancement, acceleration with a separate ME module and integration into an encoder or a decoder. The computational cost was measured in terms of average time spent on enhancement per frame. For the cases when the enhancement was integrated into the codec, we did not count the actual encoding or decoding time, so as to measure only the enhancement itself. As shown in the Table III, using a separate ME module saved about 27.5% time on average compared with the frame-wise algorithm. On the other hand, integrating with the decoder saved 40% time compared with the frame wise algorithm, while integrating with the encoder saved about 77.3%.

VI. CONCLUSIONS

In the paper, we propose a novel fast and efficient integrated algorithm for real-time enhancement of videos acquired under challenging lighting conditions including low lighting, bad weather (hazy, rainy, snowy) and high dynamic range conditions. We show that visually and statistically, hazy video and video captured in various challenging lighting conditions are very similar, and therefore a single core enhancement algorithm can be utilized in all cases, along with a proper pre-processing and an automatic impairment source detection module. We also describe a number of ways of reducing the computational complexity of the system while maintaining good visual quality, and the tradeoffs involved when the proposed system is integrated into different modules of the video acquisition, coding, transmission and consumption chain.

Areas of further improvements include better pre-processing filters targeting specific sources of impairments, improved core enhancement algorithm, and better acceleration techniques. Also of great importance is a system that can process inputs with compounded impairments (e.g. video of foggy nights, with both haze and low lighting).

TABLE III
PROCESSING SPEEDS OF PROPOSED ALGORITHMS OVER PC AND IPHONE4

	PC/ms per frame	iPhone4/ms per frame	Time saved
Frame-wise enhancement algorithm	40.1	500.3	N/A
Separate ME acceleration enhancement algorithm	29.3	369	27.5%
Integration of ME acceleration enhancement algorithm into encoder	9.2	107.9	77.3%
Integration of ME acceleration enhancement algorithm into decoder	24.8	302.4	40.0%



Fig. 17. Examples of haze removal algorithm: Original input (Top), and the enhancement result (Bottom).



Fig. 18. Examples of rainy video enhancement using haze removal algorithm: Original input (Top), and the enhancement result (Bottom).

VII. ACKNOWLEDGMENTS

The authors wish to thank the SRT students Yao Lu, Wei Meng, Yuanjie Liu, Huan Jing and Xuefeng Hu at the Media Lab of the Department of Computer Science and Technology of Tsinghua University for the help they provided to this paper.

REFERENCES

- [1] M. Blanco, H. M. Jonathan, and T. A. Dingus. "Evaluating New Technologies to Enhance Night Vision by Looking at Detection and Recognition Distances of Non-Motorists and Objects," in *Proc. Human Factors and Ergonomics Society*, Minneapolis, MN, Jan. 2001, vol. 5, pp. 1612-1616.
- [2] O. Tsimhoni, J. Bärgrman, T. Minoda, and M. J. Flannagan. "Pedestrian Detection with Near and Far Infrared Night Vision Enhancement," Tech. rep., The University of Michigan, 2004.
- [3] L. Tao, H. Ngo, M. Zhang, A. Livingston, and V. Asari. "A Multi-sensor Image Fusion and Enhancement System for Assisting Drivers in Poor Lighting Conditions," in *Proc. IEEE Conf. Applied Imagery and Pattern Recognition Workshop*, Washington, DC, Dec. 2005, pp. 106-113.
- [4] H. Ngo, L. Tao, M. Zhang, A. Livingston, and V. Asari. "A Visibility Improvement System for Low Vision Drivers by Nonlinear Enhancement of Fused Visible and Infrared Video," in *Proc. IEEE Conf. Computer Vision and Pattern Recognition*, San Diego, CA, Jun. 2005, pp.25.
- [5] H. Malm, M. Oskarsson, E. Warrant, P. Clarberg, J. Hasselgren, and C. Lejdfors. "Adaptive Enhancement and Noise Reduction in Very Low Light-Level Video," in *Proc. IEEE Int. Conf. Computer Vision*, Rio de Janeiro, Brazil, Oct. 2007, pp. 1-8.
- [6] E. P. Bennett, L. McMillan. "Video Enhancement Using Per-pixel Virtual Exposures," in *Proc. SIGGRAPH '05*, Los Angeles, CA, Jul. 2005, pp. 845-852.
- [7] Koschmieder. "Theorie der horizontalen sichtweite," in *Beitr. Phys. Freien Atm.*, vol. 12, pp. 171-181, 1924.
- [8] R. Lim, T. Bretschneider. "Autonomous Monitoring of Fire-related Haze from Space," in *Conf. Imaging Science, Systems and Technology*, Las Vegas, Nevada, Jun. 2004, pp. 101-105.
- [9] C. Song, C. E. Woodcock, K. C. Seto, M. P. Lenney, and S. A. Macomber. "Classification and Change Detection Using Landsat TM Data: When and How to Correct Atmospheric Effects?" in *Int. Symposium Remote Sensing of Environment.*, vol. 75, no. 2, pp. 230-244, Feb. 2001.
- [10] Du Y., Guindong B., and Cihlar J.. "Haze Detection and Removal in High Resolution Satellite Image with Wavelet Analysis," in *IEEE Trans. Geoscience and Remote Sensing*, vol. 40, no. 1, pp. 210-217, Jan. 2002.
- [11] R.A. Fisher, and F. Yates. "Statistical Tables for Biological, Agricultural and Medical Research," in 6th Ed. Oliver and Boyd, Ltd., Edinburgh and London, 1963, pp. 10-30.
- [12] K. He, J. Sun, and X. Tang. "Single Image Haze Removal Using Dark Channel Prior," in *Proc. IEEE Conf. Computer Vision and Pattern Recognition*, Miami, FL, Jun. 2009, pp. 1956-1963.
- [13] R. Fattal. "Single Image Dehazing," in *Proc. SIGGRAPH '08*, Los Angeles, CA, Aug. 2008, pp. 1-9.
- [14] R. Tan. "Visibility in Bad Weather from A Single Image," in *Proc. IEEE Conf. Computer Vision and Pattern Recognition*, Anchorage, Alaska, Jun. 2008, pp. 1-8.
- [15] S. G. Narasimhan, and S. K. Nayar. "Chromatic Framework for Vision in Bad Weather," in *Proc. IEEE Conf. Computer Vision and Pattern Recognition*, Hilton Head, SC, Jun. 2000, vol. 1, pp. 1598-1605.
- [16] A. M. Tourapis. "Enhanced Predictive Zonal Search for Single and



Fig. 19. Examples of snowy video enhancement using haze removal algorithm: Original input (Top), and the enhancement result (Bottom).

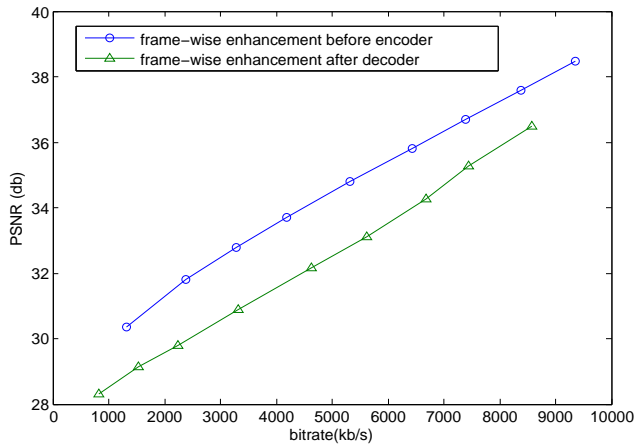


Fig. 20. RD performance of frame-wise enhancement in encoder and decoder.

- Multiple Frame Motion Estimation,” in *Proc. Visual Communications and Image Processing*, San Jose, CA, Jan. 2002, pp. 1069-1079.
- [17] T. Koga, K. Inuma, A. Hirano, Y. Iijima, and T. Ishiguro. “Motion Compensated Interframe Coding for Video Conferencing,” in *Proc. Nat. Telecommun. Conf.*, New Orleans, LA, Nov. 1981, pp. G5.3.1-G5.3.5.
- [18] B. Girod, and K. W. Stuhlmüller. “A Content-Dependent Fast DCT for Low Bit-Rate Video Coding,” in *Proc. IEEE Int. Conf. Image Process.*, Chicago, Illinois, Oct. 1998, vol. 3, pp. 80-83.
- [19] X. Dong, Y. Pang, and J. Wen. “Fast Efficient Algorithm for Enhancement of Low Lighting Video,” *SIGGRAPH '10 Poster*, Los Angeles, CA, Jul. 2010.
- [20] X. Dong, Y. Pang, J. Wen, G. Wang, W. Li, Y. Gao, and S. Yang. “A Fast Efficient Algorithm for Enhancement of Low Lighting Video,” in *Int. Conf. Digital Media and Digital Content Management*, Chongqing, China, Dec. 2010.

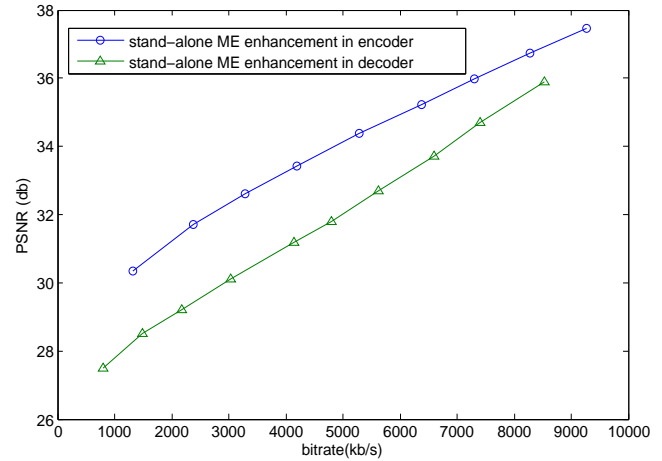


Fig. 21. RD performance of separate ME acceleration enhancement in encoder and decoder.

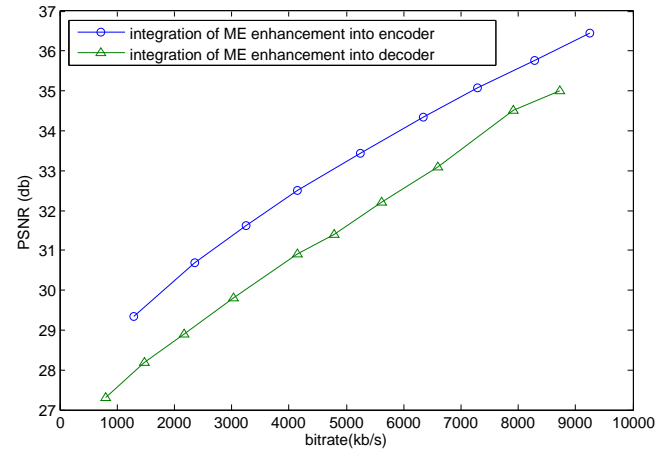


Fig. 22. RD performance of integration of ME acceleration enhancement into encoder and decoder.



Fig. 23. Examples of comparisons among the frame-wise algorithm and the three proposed ME acceleration methods: Original input (Top left), output of frame-wise algorithm (Top middle), output of separate ME acceleration algorithm (Top right), output of integration of ME acceleration algorithm into encoder (Bottom left) and decoder (Bottom right).